Published in final edited form as:
Sci Transl Med. 2012 July 11; 4(142): 142ra95. doi:10.1126/scitranslmed.3004062.

Matrix Metalloproteinase Induction of Rac1b, a Key Effector of Lung Cancer Progression

Melody L. Stallings-Mann[1,*], **Jens Waldmann**[1,2], **Ying Zhang**[1], **Erin Miller**[1], **Mona L. Gauthier**[3], **Daniel W. Visscher**[4], **Gregory P. Downey**[5,6,7], **Evette S. Radisky**[1], **Alan P. Fields**[1], and **Derek C. Radisky**[1,*]

[1]Department of Cancer Biology, Mayo Clinic Cancer Center, Jacksonville, FL 32224, USA

[2]Department of Visceral, Thoracic, and Vascular Surgery, University Hospital Giessen and Marburg, Marburg, Baldingerstrasse 35043, Germany

[3]Campbell Family Institute for Cancer Research, Ontario Cancer Institute, Toronto, Ontario M5G 2C1, Canada

[4]Department of Anatomic Pathology, Mayo Clinic Cancer Center, Rochester, MN 55906, USA

[5]Division of Pulmonary Sciences and Critical Care Medicine, Department of Medicine, University of Colorado Denver, Aurora, CO 80045, USA

[6]Department of Pediatrics, University of Colorado Denver, Aurora, CO 80045, USA

[7]Integrated Department of Immunology, National Jewish Health and University of Colorado Denver, Aurora, CO 80045, USA

[*]To whom correspondence should be addressed. stallingsmann.melody@mayo. edu (M.L.S.-M.); radisky.derek@mayo.edu (D.C.R.).

Author contributions: M.L.S.-M., J.W., M.L.G., E.S.R., A.P.F., and D.C.R. designed the experiments; M.L.S.-M., J.W., Y.Z., E.M., and D.C.R. performed the experiments; M.L.S.-M., J.W., M.L.G., D.W.V., G.P.D., E.S.R., A.P.F., and D.C.R. interpreted the experiments and assembled the figures; M.L.S.-M. and D.C.R. wrote the manuscript; and all authors participated in editing and refinement of the manuscript.

Competing interests: The authors declare that they have no competing financial interests.

SUPPLEMENTARY MATERIALS
www.sciencetranslationalmedicine.org/cgi/content/full/4/142/142ra95/DC1
Materials and Methods
Fig. S1. Expression of Rac1b mRNA in human lung adenocarcinoma homogenates.
Fig. S2. Altered expression of mesenchymal and epithelial markers in *CCSP-rtTA/tet-Rac1b* transgenic mouse tumors.
Fig. S3. Coexpression of *Rac1b* transgene and vimentin in *CCSP-rtTA/tet-Rac1b* transgenic mouse tumors.
Fig. S4. Expression of Rac1b protein is inhibited by siRNA for Rac1b in H661 cells.
Fig. S5. Classification of neoplasms in mouse lung.
Fig. S6. Adenocarcinoma from a urethane-treated *tetO-HA-MMP-3/CCSP-rtta* bitransgenic mouse.
Fig. S7. Coexpression of the *tetO-HA-MMP-3* transgene and the mesenchymal protein vimentin.
Fig. S8. Gene expression profiles of RNA isolated from lungs of *tetO-HA-MMP-3/CCSP-rtta* or *CCSP-rtta* mice treated with urethane and exposed to doxycycline.
Fig. S9. Induction of morphological alterations in primary lung epithelial cells by transgenic expression of MMP-3.
Fig. S10. Progression to adenocarcinoma in *tetO-HA-MMP-3/CCSP-rtta* mice in the urethane-induced tumorigenesis model.
Fig. S11. Decrease in expression of senescence markers upon MMP-3 expression in *tetO-HA-MMP-3/CCSP-rtta* mouse lung tissue in the urethane-induced tumorigenesis model.
Fig. S12. Potentiation of tumor formation in *K-Ras*^{LA2} mice by expression of MMP-3.
Fig. S13. Immunohistochemical analyses of paraffin-embedded tissues with primary antibodies.
Data set S1. Genes that differ more than twofold in any condition in lung tissue homogenates from *tetO-HA-MMP-3/CCSP-rtta* and control mice (Excel file).
Data set S2. Genes that are differentially expressed ($P < 0.05$) in lung tissue homogenates in *tetO-HA-MMP-3/CCSP-rtta* versus control mice (Excel file).
Data set S3. Gene ontology analysis of differentially expressed genes ($P < 0.05$) from lung tissue homogenates of *tetO-HA-MMP-3/CCSP-rtta* versus control mice (Excel file).

Abstract

Lung cancer is more deadly than colon, breast, and prostate cancers combined, and treatment improvements have failed to improve prognosis significantly. Here, we identify a critical mediator of lung cancer progression, Rac1b, a tumor-associated protein with cell-transforming properties that are linked to the matrix metalloproteinase (MMP)–induced epithelial-mesenchymal transition (EMT) in lung epithelial cells. We show that expression of mouse Rac1b in lung epithelial cells of transgenic mice stimulated EMT and spontaneous tumor development and that activation of EMT by MMP-induced expression of Rac1b gave rise to lung adenocarcinoma in the transgenic mice through bypassing oncogene-induced senescence. Rac1b is expressed abundantly in stages 1 and 2 of human lung adenocarcinomas and, hence, is an attractive molecular target for the development of new therapies that prevent progression to later-stage lung cancers.

INTRODUCTION

A devastating disease that affects millions of people each year, lung cancer is the second highest cause of morbidity and mortality worldwide. Non–small cell lung cancers (NSCLCs) represent more than 80% of all cases (1), and exposure to cigarette smoke dominates as the causative agent. Recent advances in early detection of lung cancer have made substantial progress in reducing mortality (2), but gaps in our knowledge about the molecular mechanisms of pathogenesis and the biological characteristics of lung cancers form barriers to the development of more effective targeted therapies. It is imperative that we improve our understanding of the disease mechanisms to identify new therapeutic targets and strategies for treatment.

Rac1b is an alternatively spliced isoform of Rac1, a Rho family guanosine triphosphatase (GTPase) that is known to regulate diverse cellular processes, such as actin cytoskeleton organization, membrane trafficking, cell proliferation, and gene expression (3-6). The Rac1b isoform results from inclusion of exon 3b, which contains 57 nucleotides and leads to a 19–amino acid in-frame insertion (7, 8). The resulting protein has accelerated guanosine diphosphate (GDP)/guanosine triphosphate (GTP) exchange and impaired GTP hydrolysis (9, 10), which lead to a predominance of the GTP-bound form in the cellular context and associated prolonged signaling activity (9). Rac1b shows increased expression in malignant colorectal (7) and breast cancer (8), and studies with cultured cells have shown that Rac1b may exert oncogenic activities through induction of mitochondrial reactive oxygen species (ROS) production and consequent promotion of the epithelial-mesenchymal transition (EMT) (11).

EMT is a phenotypical alteration in which epithelial cells detach from their neighbors and the underlying basement membrane and become more motile and invasive (12, 13). In cultured cells, EMT can be induced by cytokines, growth factors, and proteases (14). Matrix metalloproteinases (MMPs)—zinc-requiring enzymes that reside in and degrade components of the extracellular matrix—have been shown to induce EMT; MMP-3, MMP-7, and MMP-28 induce EMT in human A549 lung adenocarcinoma (LAC) cells (15-17), and MMP-3 also induces EMT in both mouse mammary epithelial cells (11, 18) and human breast cancer cells (19). Although MMPs are known to function in lung embryonic development and in lung cancer progression (20), the involvement of MMP-induced EMT in lung cancer has not been defined.

A major barrier to tumor progression is oncogene-induced senescence (OIS), a $p19^{Arf}$–p53/$p16^{Ink4a}$–retinoblastoma protein–dependent mechanism that limits the proliferative capacity of premalignant cells and that has been best defined for the transition from premalignant lung adenoma to malignant LAC (21). Recent studies indicate that aberrant expression of the

EMT-associated transcription factor Twist in cultured cells allows the cells to bypass OIS (22), suggesting that induction of EMT at an early stage of tumor development might stimulate progression from adenoma to carcinoma in vivo. Here, we use cell culture and mouse models in which the role of OIS in tumor progression has been well defined in combination with new transgenic mouse models that display MMP-inducible mouse Rac1b expression and signaling to show that (i) Rac1b functions as a lung cancer oncogene in mice and humans, (ii) expression of MMPs in lung tissue leads to activation of Rac1b, and (iii) activation of EMT by MMP-induced expression of Rac1b stimulates bypass of OIS and progression to LAC.

RESULTS

Association of increased Rac1b expression with LAC

Evaluation of a panel of LAC biopsies and adjacent normal tissue samples enriched in patients with stage 1 and stage 2 disease revealed that Rac1b mRNA expression was significantly up-regulated ($P < 0.0001$, unpaired t test) in LAC compared to that in normal adjacent tissue (Fig. 1A and fig. S1, A and B); furthermore, Rac1b mRNA expression was increased in stage 2 relative to stage 1 disease (Fig. 1B), suggesting the involvement of Rac1b during the early stages of lung cancer progression. Using immunohistochemistry (IHC), we found consistently high expression of the Rac1b protein in adenocarcinoma tumor cells (Fig. 1C), indicating a potentially direct role for Rac1b in tumor cell progression. We also found that Rac1b mRNA was significantly increased ($P = 0.0238$, unpaired t test) in primary tumors of patients who showed node positivity relative to tumors in patients with node-negative disease, suggesting a potential link between expression of Rac1b and spread beyond the primary tumor site (Fig. 1D). Because cigarette smoke is a major lung cancer carcinogen, we evaluated Rac1b expression in association with smoking status in patients. Nonmalignant adjacent lung tissue from patients who were current smokers had significantly ($P = 0.011$, unpaired t test) higher expression of Rac1b than normal adjacent lung tissue from patients who were never smokers (Fig. 1E). To assess whether there is a relationship with Rac1b status in emphysematous lung disease, we assessed Rac1b expression in a cohort of patients diagnosed with idiopathic pulmonary fibrosis and found that those with peripheral or subpleural distribution of emphysema had significantly higher ($P < 0.05$, Mann-Whitney test) expression of Rac1b compared to patients who had no axial distribution of emphysema (Fig. 1, F and G).

To define the role of Rac1b in induction of EMT and lung cancer in vivo, we created bitransgenic mice with inducible expression of Rac1b in lung epithelial cells. *tetO-YFP-Rac1b* transgenic mice were crossed with mice bearing the *CCSP-rtta* activator transgene, which expresses the reverse tetracycline transactivator (rtTA) under the control of the Clara cell secretory protein (CCSP) promoter (23). Through quantitative polymerase chain reaction (qPCR) analysis of transgene expression, two stable transgenic mouse lines were identified, designated A and F. Expression of the transgene was selectively induced in lung but not liver by feeding the mice doxycycline (Fig. 2, A and B). IHC performed with an antibody specific for the insertion sequence of the Rac1b isoform (11) showed typical CCSP-driven expression patterns (Fig. 2C) (23). Transgene expression progressively increased when mice were fed larger doses of doxycycline (Fig. 2D). Exogenous expression of Rac1b in cultured epithelial cells results in the activation of cells with characteristics of myofibroblasts (12, 14, 24, 25), which are key effector cells in the development of tissue fibrosis—an accumulation of collagen fibrils that can disrupt tissue structure and significantly increase risk of tumor development (12). Thus, we examined *tetO-YFP-Rac1b/CCSP-rtta* mice fed doxycycline and found that dose-dependent expression of Rac1b in airway epithelial cells was accompanied by the development of peri-airway fibrosis, increased collagen expression, and deposition of collagen fibrils (Fig. 2E). These results

reveal that even short-term expression of Rac1b causes alterations in tissue architecture consistent with activation of EMT.

Persistent fibrosis has been linked to an increased risk of tumor development (25); thus, we evaluated spontaneous tumor formation in *tetO-YFP-Rac1b/CCSP-rtta* lines A and F, which express differential amounts of the transgene (Fig. 2F), and in *CCSP-rtta* control mice maintained on a doxycycline diet for an extended time. A single adenoma was detected in the lungs of *CCSP-rtta* control mice ($n = 6$), consistent with previous reports of sporadic lung adenoma formation in wild-type Friend virus B-type (FVB) strain mice (26). However, numerous tumors were detected in the lungs of 7 of 16 *tetO-YFP-Rac1b/CCSP-rtta* mice, with 4 of 16 containing multiple tumors (Fig. 2G). Many of these tumors had progressed to adenocarcinoma (Fig. 2H), having features such as a tumor diameter greater than 5 mm (Fig. 2G), greater numbers of atypical and mitotic cells relative to sporadic adenomas that developed in nontransgenic mice (Fig. 2I), tumor cell invasion of large airways (Fig. 2J) and surrounding tissue (Fig. 2K), and variation in architectural growth patterns of neoplastic epithelium. Rac1b expression produced tissue fibrosis even in lungs that did not develop tumors (Fig. 2L), indicating that fibrosis preceded tumor formation. Lungs that developed spontaneous tumors also showed significantly increased expression of Rac1b ($P < 0.01$, Mann-Whitney test) as well as increased expression of mesenchymal marker transcripts, including smooth muscle actin ($P < 0.01$, Mann-Whitney test), collagen 1A1 ($P < 0.01$, Mann-Whitney test), and vimentin ($P < 0.05$, Mann-Whitney test; Fig. 2M). Immunohistochemical analysis of transgenic mouse lung sections identified intratumoral areas that displayed increased expression of collagen, vimentin, and α-smooth muscle actin, as well as decreased expression of epithelial markers (Fig. 2N and fig. S2), which is consistent with the possibility that an EMT-type transition had occurred within the tumors in the *tetO-YFP-Rac1b/CCSP-rtta* mice.

Progression to adenocarcinoma requires the cells to bypass senescence, which is induced by deactivation of the retinoblastoma and p53 tumor suppressor pathways (21, 27). Although activation of EMT processes was shown to stimulate bypass of Ras-induced senescence in cultured mammary epithelial cells (22), it is not clear how senescence is bypassed in vivo or which, if any, EMT processes are involved. The spontaneous adenocarcinoma formation we observed in the *tetO-YFP-Rac1b/CCSP-rtta* transgenic mice (Fig. 2) might have resulted from senescence bypass induced by Rac1b-induced EMT. To test this possibility, we treated *tetO-YFP-Rac1b/CCSP-rtta* and control *CCSP-rtta/ntg* mice with ethyl carbamate (urethane), a DNA alkylating agent present in cigarette smoke that induces lung adenomas through the generation of activated Kras protein (28). Tumors that developed in *tetO-YFP-Rac1b/CCSP-rtta* mice showed substantial expression of Rac1b protein and mRNA, as measured by IHC (Fig. 3A) and qPCR (Fig. 3B), respectively. Although the number of tumors per mouse did not significantly differ between *tetO-YFP-Rac1b/CCSP-rtta* and control mice, the average tumor size (0.47 mm^2 versus 0.37 mm^2, respectively) was significantly increased ($P < 0.05$, Mann-Whitney test; Fig. 3C) in *tetO-YFP-Rac1b/CCSP-rtta* mice, and the presence of these large and invasive tumors (Fig. 3D) indicated progression to adenocarcinoma, a phenomenon consistent with bypass of senescence. A Rac1b-induced proliferation of mesenchymal cells was evidenced by a significant increase, in *tetO-YFP-Rac1b/CCSP-rtta* mice relative to control mice, in the expression of EMT marker transcripts ($P < 0.05$, Mann-Whitney test) in whole-lung homogenates (Fig. 3E) and EMT marker proteins within tumors (Fig. 3F). Dual-fluorescence tissue-labeling experiments supported the association of Rac1b expression with the increase in mesenchymal cell components through activation of EMT: Specifically, in *tetO-YFP-Rac1b/CCSP-rtta* mice, the *tetO-YFP-Rac1b* transgene was coexpressed with the epithelial cell marker CCSP in Clara cells (Fig. 3G) in airways and with the mesenchymal marker vimentin in the lung tumors (arrowheads in Fig. 3H and fig. S3). These observations are

consistent with the interpretation that Rac1b can induce EMT in Rac1b-expressing cells. Expression of the senescence marker $p16^{Ink4a}$ (Fig. 3, I and J) was decreased, and expression of the proliferation marker Ki67 (Fig. 3K) was increased in *tetO-YFP-Rac1b/CCSP-rtta* mice relative to controls, suggesting that Rac1b-induced EMT in urethane-initiated tumors is associated with senescence bypass.

Induction of Rac1b and mesenchymal gene expression by MMPs in cultured cells

Rac1b is known to be induced by MMPs in cultured mammary epithelial cells (11, 24, 29, 30), and cigarette smoke is known to induce MMP expression in lung epithelial cells (31). Therefore, because our studies thus far implicated Rac1b in lung cancer progression, we evaluated the response of H661 human lung cancer cells, which exhibit intermediate invasiveness and malignancy (32), to a panel of recombinant MMPs. Rac1b expression was effectively induced by MMP-3 and MMP-9, but not by MMP-1 (Fig. 4A). Induction of the mesenchymal marker vimentin correlated with up-regulation of Rac1b (Fig. 4B) by these same MMPs.

MMP-3 expression has been found in respiratory epithelial cells [see the Human Protein Atlas (33)] and in lung cancer cells (34-36), and in our studies, overlapping expression of MMP-3 and Rac1b was observed in human lung cancer biopsies (Fig. 4, C and D). Because expression of MMP-3 has also been found in human lung fibrosis, an EMT-associated phenomenon (37-39), we concentrated on MMP-3 as an experimental EMT inducer and assessed a specific role for Rac1b in the increased expression of vimentin in the H661 lung cancer cells treated with MMP-3. Rac1b expression rose in a dose-dependent manner after incubation of the H661 lung cancer cells with MMP-3 (Fig. 4E); this enhanced expression was accompanied by progressively increasing expression of vimentin (Fig. 4F). Acquisition of a flattened cellular morphology (Fig. 4G) was associated with increased expression of myofibroblast-associated smooth muscle actin and, as seen previously, during the early EMT response of mammary epithelial cells to MMP-3 (24). Selective knockdown of Rac1b by small interfering RNA (siRNA) targeting of the unique 57-nucleotide insertion (Fig. 4H and fig. S4) effectively blocked MMP-3–induced expression of vimentin (Fig. 4I).

Induction of Rac1b and EMT-associated lung tumor progression by MMP-3 in vivo

To determine whether MMP-3 could increase Rac1b expression and activate EMT in vivo, we generated *tetO-HA-MMP-3* transgenic mice and crossed them with mice bearing the *CCSP-rtta* activator transgene, identifying three *tetO-HA-MMP-3/CCSP-rtta* founder lines (Fig. 5A). The *MMP-3* transgene was highly inducible by doxycycline (Fig. 5B) and was specifically expressed in the lung (Fig. 5C) in *tetO-HA-MMP-3/CCSP-rtta* mice. Control and *tetO-HA-MMP-3/CCSP-rtta* mice were treated with urethane to induce lung tumors and then with doxycycline to induce transgene expression, and multiple lesions were detected in both groups of mice. The lesions were predominantly solid and papillary adenoma, but progression to adenocarcinoma was observed in a subset of *tetO-HA-MMP-3/CCSP-rtta* mice, as indicated by tumor sizes greater than 5 mm in diameter, the presence of pleomorphic nuclei, and evidence of invasion at the tumor-host interface (Fig. 5D and figs. S5 and S6). Tumor number (Fig. 5E; $P < 0.001$, Mann-Whitney test) and size (Fig. 5F; $P < 0.05$, Mann-Whitney test) were greater in the *tetO-HA-MMP-3/CCSP-rtta* mice, indicating that MMP-3 might potentiate tumor formation as well as stimulate tumor progression. Expression of Rac1b was increased in the airways and in lung tumors of the *tetO-HA-MMP-3* transgenic mice (Fig. 5, G to I). This increase was associated with a decrease in the nuclear localization of the heterogeneous nuclear ribonucleoprotein A1 (hnRNP A1) (Fig. 5, J to M), which previously was shown to bind to exon 3b in Rac1 mRNA and to inhibit exon inclusion, thus blocking expression of Rac1b (40).

Associated with the increased tumor progression in the *tetO-HA-MMP-3/CCSP-rtta* mice, we observed increased deposition of collagen adjacent to airways, as assessed by trichrome stain; decreased expression of E-cadherin in airway epithelial cells, as assessed by IHC (Fig. 6A); and increased expression of mesenchymal marker mRNA in lung homogenates, as assessed by qPCR (Fig. 6B), all compared to control mice. The notion that these effects were associated with MMP-3–induced EMT was supported by dual-fluorescence labeling of cells adjacent to the airways, which showed coexpression of the *HA-MMP-3* transgene in vimentin-expressing cells (Fig. 6C and fig. S7). To provide a broader view of the EMT-promoting cell signaling alterations induced by MMP-3/Rac1b, we performed transcriptional profiling of RNA derived from homogenates of lung tissue isolated from *tetO-HA-MMP-3/CCSP-rtta* ($n = 3$) and control ($n = 3$) mice. We found that 6361 transcripts showed expression changes greater than twofold in *tetO-HA-MMP-3/CCSP-rtta* versus control mice, and clustering analysis efficiently segregated the controls from the MMP-3–expressing bitransgenic mice (annotated gene expression data are shown in data set S1). This segregation led to the identification of 2948 transcripts that were differentially expressed between control and bi-transgenic mice [$P < 0.05$ by analysis of variance (ANOVA)] (annotated expression data are shown in data set S2). Gene ontology analyses showed specific up-regulation of transcripts associated with lung development ($P = 0.00707$), response to oxidative stress ($P = 0.0018$), and alveolar liquid surface tension ($P = 2.67 \times 10^{-7}$; all categories with significant overlap are presented in data set S3). We subjected the list of differentially expressed genes to a NextBio meta-analysis (41) and found significant overlap with differentially expressed genes in four experimental data sets (for all analyses, $P < 0.0001$); these studies assessed cigarette smoke–induced effects in human bronchial epithelial cell lines (42), mice exposed to cigarette smoke (43), airway epithelial cells from smokers versus nonsmokers (44), and LAC samples from smokers versus nonsmokers (45) (fig. S8). Significance was found for overlap of our data set with each of these, indicating a possible role for MMP/Rac1b-induced signaling in cigarette smoke–induced pathologies. These findings are consistent with several previous studies showing MMP up-regulation in response to cigarette smoke (31).

To determine whether MMP-3 could induce EMT-like changes in primary lung epithelial cells, we isolated alveolar epithelial cells from transgenic mice that expressed either yellow fluorescent protein (YFP) under the control of the collagen A1 promoter (col-YFP) or red fluorescent protein (RFP) under the control of the smooth muscle actin promoter (sma-RFP; a gift from D. Brenner), plated them on three-dimensional Matrigel to maintain tissue-specific characteristics (46), and supplemented the medium with recombinant MMP-3. These experiments showed activation of fluorescence in cells treated with recombinant MMP-3 relative to untreated cells (Fig. 6, D and E). Primary alveolar epithelial cells isolated from nontransgenic wild-type mice and treated with recombinant purified MMP-3 showed decreased expression of the lung Clara cell differentiation marker CCSP and increased expression of the myofibroblast markers smooth muscle actin and vimentin (Fig. 6F), indicating an MMP-3–induced EMT. To determine whether transgenic MMP-3 could induce EMT-like changes, we isolated primary alveolar epithelial cells from *tetO-HA-MMP-3/CCSP-rtta* transgenic mice and cultured the cells on Matrigel to maintain tissue-specific gene expression without addition of exogenous MMP-3; addition of increasing amounts of doxycycline to the culture stimulated a progressive invasive branching phenotype (Fig. 6G and fig. S9) characteristic of the development of contractility. To study these effects in vivo, we instilled the lungs of col-YFP/sma-RFP double-transgenic mice with one of three adenoviral vectors, ad-LacZ, ad-MMP-3, or ad-TGFβ (transforming growth factor–β), which expressed either the *LacZ* (control), the *MMP-3*, or the *TGFβ*, respectively (39). We observed a fibrotic reaction after 3 weeks in the MMP-3– and TGFβ-expressing mice (Fig. 6H) and found that, when analyzed by flow cytometry, isolated primary alveolar epithelial cells from ad-MMP-3– or ad-TGFβ–treated mice revealed an increased number of cells that

expressed both the YFP and the RFP markers compared to control animals that received ad-LacZ (Fig. 6I). These results support the conclusion that MMP-3/Rac1b–induced changes in cell signaling drive alveolar epithelial cells to undergo EMT toward a myofibroblast phenotype.

MMP-3/Rac1b-induced bypass of oncogene-associated senescence in mouse lung adenomas

To define the stage of tumor progression during which MMP-3 and Rac1b exert their influence, we evaluated the effects of MMP-3 induction at either the time of weaning, the time of urethane injection, or 3 weeks after urethane injection and then stopped MMP-3 expression at either the time of urethane injection, 3 weeks after urethane injection, or at harvest (Fig. 6J). Comparison of tumors in mice that expressed MMP-3 during the tumor initiation period (weeks 1 to 3) with those from mice that expressed MMP-3 during tumor progression (weeks 3 to 14) revealed that tumor size was significantly increased in *tetO-HA-MMP-3/CCSP-rtta* mice only when MMP-3 expression was initiated after the urethane treatment and then maintained until organ harvest (Fig. 6, K and L). Tumors in hematoxylin and eosin (H&E)–stained lung sections were scored for atypical adenomatous hyperplasia (AAH), adenoma, and adenocarcinoma, and we found adenocarcinoma formation only in mice treated with doxycycline, and thus expressing MMP-3, continuously until the time of harvest (Fig. 6M). Thus, expression of MMP-3 specifically during tumor progression promotes adenocarcinoma. When three additional MMP-3 founder lines were treated with urethane and fed doxycycline from the time of urethane injection until harvest, adenocarcinoma formation was observed in these lines as well (fig. S10). We conclude that MMP-3 expression does not alter response to urethane but acts as a promoter of tumor progression, consistent with EMT-associated senescence bypass.

To further define the MMP-3/Rac1b–associated bypass of Kras-induced senescence, we performed IHC to detect (OIS) markers—p15/INK4B, p16/INK4A, and tumor necrosis factor receptor superfamily member decoy receptor (DCR2) (21)—and one proliferation marker, Ki67, in serial lung sections from urethane-treated *tetO-HA-MMP-3/CCSP-rtta* or *CCSP-rtta/ntg* mice fed doxycycline to induce transgene and thus MMP-3 expression. The staining intensity of p15/INK4B and DCR2 was significantly lower in lung tumors from *tetO-HA-MMP-3/CCSP-rtta* mice (Fig. 6N and fig. S11) relative to control *CCSP-rtta/ntg* mice, which is consistent with bypass of senescence. Tumors that showed intense staining for all four OIS markers were not detected in *tetO-HA-MMP-3/CCSP-rtta* mice, whereas they were readily observed in control mice (Fig. 6N). In contrast, most tumors in *tetO-HA-MMP-3/CCSP-rtta* mice showed little to no staining of OIS markers accompanied by a higher percentage of nuclei positive for the cell proliferation marker Ki67 relative to control mice (Fig. 6N). These data indicate that expression of MMP-3 could act as a tumor promoter by causing urethane-induced adenomas to develop to adenocarcinoma through bypass of OIS. Under conditions of extended transgene expression, MMP-3/Rac1b may also function in cell transformation. We previously observed in mouse mammary cell models that MMP-3–induced Rac1b can spur genomic instability (11) and cannot rule out a potential role for MMP-3/Rac1b in a similar process in lung.

To evaluate potentiation of tumor development by MMP-3 in mice with a specific activating mutation of Kras, we performed a series of parallel experiments using mouse strains that carry an oncogenic allele of *KRAS* (*Kras*^{LA2}) that can be activated by spontaneous recombination and are highly predisposed to early-onset lung cancer (47). Triple-transgenic (*tetO-HA-MMP-3/CCSP-rtta/Kras*^{LA2}) and control (*CCSP-rtta/Kras*^{LA2} or *ntg/Kras*^{LA2}) mice were fed doxycycline continuously from the time of weaning until harvest 14 weeks later. The triple-transgenic mice that expressed MMP-3 had numerous lesions visible in the lung (fig. S12A), with increased tumor number (fig. S12B; $P < 0.05$, Mann-Whitney test)

and size (fig. S12C; $P < 0.001$, Mann-Whitney test) as well as increased expression of Rac1b (fig. S12D; $P < 0.05$, Mann-Whitney test) relative to MMP-3–expressing control mice. Consistent with a bypass of Kras-induced senescence, the MMP-3–expressing triple-transgenic mice displayed decreased expression of $p16^{Ink4a}$ and increased proliferation (as assessed by Ki67 expression; fig. S11E) compared to control mice. We thus conclude that MMP-3 can drive tumor progression in $Kras^{LA2}$ mutant mice.

DISCUSSION

Increased expression of MMPs is found in nearly every tumor type, and specific MMPs have been associated with many aspects of tumor biology, including tissue invasion, metastasis, and neoangiogenesis. Our results provide insight into a new mechanism by which MMP expression can promote tumor progression. In previous studies using cultured mammary epithelial cells, we demonstrated that treatment with MMP-3 stimulated induction of Rac1b and consequent activation of the EMT transcriptional program (11). Herein, we have identified Rac1b as an inducer of EMT in vivo and as a key intermediate in MMP-induced lung cancer progression. The EMT program can be initiated by a variety of intrinsic signals (for example, gene mutations) or extrinsic signals (such as growth factor signaling). Because EMT characteristics are now being recognized in human cancers, there is an increasing emphasis toward identifying therapeutic approaches that target EMT. It has been shown that the cellular changes associated with EMT-like transitions alter the dependence of carcinoma cells on epidermal growth factor receptor (EGFR) signaling networks and are associated with NSCLC tumor cell, xenograft, and patient insensitivity to selective EGFR tyrosine kinase inhibitors (TKIs) (48-50). Novel therapeutics that inhibit pathological inducers of EMT may sensitize tumor cells and enhance response to existing therapies, whereas new therapies that are targeted specifically against downstream EMT-directed pathways might independently reduce tumor progression and metastasis of lung cancer.

Rac1b, in particular, shows promise as a point of therapeutic intervention. In cultured cells, Rac1b displays many of the properties of GTPase-deficient Rac1 mutants, but the presence of a 19–amino acid insertion enables Rac1b to interact with a distinct set of effector proteins, potentially contributing to loss of the epithelial phenotype (10, 51-53). From the viewpoint of therapeutic targeting, Rac1b has been identified uniquely in tumors and cancer cell lines and has no known functions in physiological tissue homeostasis. In addition, it seems likely that the unique structural and dynamic properties conferred by the 19–amino acid insertion may also offer the opportunity for selective targeting of Rac1b in preference to Rac1 by novel small-molecule or protein therapeutics that block EMT-associated progression to advanced tumor stages.

EMT is a physiological process best described in embryonic development (54). Although physiological activation of the complete EMT program is a highly coordinated process involving multiple mediators, there is an increasing consensus that aberrant activation of EMT inducers in the tumor microenvironment can stimulate aspects of the EMT program that drive tumor progression (55). Early investigations into this process have focused on how acquisition of motility characteristics facilitates tumor metastasis; however, other consequences of EMT induction have also been identified, including development of fibrosis, increased resistance to apoptosis, and the markedly enhanced tumorigenic potential of the cancer stem cell phenotype (56, 57). Production of myofibroblasts by EMT can also result in a stiffened extracellular matrix, which can potentiate tumor progression by disrupting tissue structure and activating cellular invasiveness (58). Experiments in cultured cells have indicated that EMT mediators could induce bypass of senescence (22), but previous studies did not indicate whether or when this process might happen in vivo. Our results implicate EMT-induced senescence bypass as a key step in lung cancer progression

and identify Rac1b as a key mediator of this process. Furthermore, our findings that Rac1b is expressed in stages 1 and 2 of lung tumor progression (Fig. 1, A and B) and in response to cigarette smoke (Fig. 1, E and G) combined with the similarities between MMP-3/Rac1b-induced molecular alterations in transgenic mice and lung tissue from human smokers (fig. S8) indicate that cigarette smoke–induced changes in lung tissue that drive lung cancer may occur through MMP-induced Rac1b. Our new experimental models allow for the development of new therapeutic strategies that target these processes.

MATERIALS AND METHODS

Generation and breeding of transgenic mice

tetO-HA-MMP-3 mice were engineered by cloning the coding sequence of *MMP-3* (59) downstream of the Tet operator in pTet-Splice (Promega). *tetO-YFP-Rac1b* mice were similarly engineered with the coding sequence of *Rac1b* (11). *tetO-HA-MMP-3* and *tetO-YFP-Rac1b* founder lines were generated by pronuclear injection into FVB mouse oocytes by standard transgenic procedures (Mayo Transgenic Core). Mice were maintained as heterozygotes by breeding with nontransgenic FVB mice (The Jackson Laboratory). Transgenic mice bearing the *tetO-YFP-Rac1b* or *tetO-HA-MMP-3* transgenes had no detectable tissue pathologies and survived normally in the vivarium. To produce mice with regulatable MMP-3 or Rac1b production, we mated *tetO-HA-MMP-3* or *tetO-YFP-Rac1b* transgenic mice with FVB mice bearing the *CCSP-rtta* activator transgene (obtained from J. Whitsett) that express the rtTA under the control of the rat CCSP (rCCSP) promoter (23). For urethane treatment, 6-week-old mice were weighed and given a single intra-peritoneal injection of 25 mg of urethane (300 μl of an 83.3 mg/ml solution; Sigma) for an approximate dose of 200 mg/kg. The injection was repeated (20 mg) on a weekly basis for 2 or 5 weeks as indicated. At either 14 or 20 weeks after injection, mice were euthanized by CO_2 asphyxiation. The lungs were removed, formalin-fixed, and paraffin-embedded. Because significant gender differences have been observed in response to urethane (60-62), results presented are for male mice only.

Animal use and administration of doxycycline

The mice were housed in pathogen-free conditions according to protocols approved by the Institutional Animal Care and Use Committee at Mayo Clinic. For induction of *tetO-HA-MMP-3* and *tetO-YFP-Rac1b* transgene expression in double-transgenic animals, the mice were fed doxycycline (Bio-Serv) at a concentration of 200 mg/kg.

Histology and IHC

Mice were euthanized, and the lungs were removed intact and fixed overnight in 10% buffered formalin. For histological analysis, lungs were embedded in paraffin, serially sectioned (5 μm), and stained with H&E. For IHC, sections were deparaffinized by placing slides into three changes of xylene and rehydrated in a graded ethanol series. The rehydrated tissue samples were rinsed in water, and most sections were subjected to heat antigen retrieval as described by the manufacturer (Dako) at either standard pH (6.9) or high pH (9.0). Slides were incubated with the appropriate primary antibody (see Supplementary Materials and Methods) with anti-rabbit–labeled polymer–horseradish peroxidase (HRP) (Dako) or, for anti-Ki67, the Rat-on-Mouse HRP Kit (Biocare).

Mouse pulmonary lesions were classified according to the recommendations of Nikitin *et al.* (63). AAH was identified as focal and diffuse lesions consisting of relatively uniform atypical cuboidal to columnar cells with dense chromatin. Lesions with well-circumscribed areas smaller than 5 mm in diameter were considered adenomas. Adenomas were categorized as solid (no evidence of papillary structures), mixed (both papillary and solid

structures present), or papillary (consists primarily of papillary structures lined by cuboidal to columnar cells). Adenocarcinomas showed greater cytological atypia, increased frequency of mitoses, regional variation in growth pattern, more papillary structures, size greater than 5 mm in diameter, and invasion of vessels or large airways.

Cell culture and reagents

The human H661 large cell lung cancer line was obtained from the American Type Culture Collection and maintained as suggested by the supplier. Methods for selective siRNA knockdown of Rac1b were described previously (11).

Type II cell isolation and culture

Murine alveolar epithelial type II cells were isolated from adult double-transgenic *tetO-HA-MMP-3/CCSP-rtta* mice (6 to 12 weeks old) following the method of Rice *et al.* (64) and were cultured on tissue culture plates coated with Matrigel (BD Biosciences). Cells were maintained in bronchial epithelial cell growth medium (BEGM; Clonetics) with 5% charcoal- and dextran-treated fetal bovine serum (FBS) in the presence or absence of doxycycline hydrochloride (Sigma) in a 37°C, 5% CO_2 incubator. Branching morphogenesis was assessed as the fraction of cell clusters per field with two or more extensions longer than the diameter of the central cell cluster.

Processing and analysis of human lung cancer tissues

Lung tumor tissues were analyzed by a pathologist to confirm initial diagnosis, staging, and overall integrity of the tissue samples. Seventy-four cases of NSCLC [37 LAC and 37 squamous cell carcinoma (SCC)] were chosen for extraction of RNA. Total RNA was isolated from cryostat sections of tumor and matched normal lung tissue with the RNAqueous-4PCR kit (Ambion). Reverse transcription–qPCR (RT-qPCR) analysis was performed on a 7900 HT Thermocycler (Applied Biosystems) with TaqMan Master Mix and primers for 18*S* complementary DNA (cDNA) purchased from Applied Biosystems. The primer/probe set for the human Rac1b transcript was a custom assay (forward primer, 5′-TATGACA-GATTACGCCCCCTATC-3′; reverse primer, 5′-CTTTGCCCCGGGA-GGTTA-3′; and probe, 5′-AAACGTACGGTAAGGAT-3′).

Enumeration and measurement of lung tumors

One central 5-μm section of each set of paraffin-embedded lungs was stained by H&E. Digital images of each lung section were captured with the Aperio ScanScope XT slide scanner (Aperio Technologies), and tumors were countered, measured, and categorized according to morphology (63).

Supplementary Material

Refer to Web version on PubMed Central for supplementary material.

Acknowledgments

We thank J. Campisi and J. P. Kirkland for helpful discussions, A. Hockla and J. Robinson for MMP enzyme preparations, D. Khauv for assistance with figures, and B. Edenfield for immunohistochemical analysis of lung tissues.

Funding: This work was supported by grants from the National Cancer Institute (CA122086 to D.C.R., CA128660 to C.M.N. and D.C.R., and CA081436 to A.P.F.) and the National Heart, Lung, and Blood Institute (HL090669 to G.P.D.), the James and Esther King Foundation (to A.P.F., D.C.R., and E.S.R.), funds from the Harold and Mary Zirin Chair in Pulmonary Biology at National Jewish Health, and the Monica Flynn Jacoby Professorship (to A.P.F.).

REFERENCES AND NOTES

1. Molina JR, Yang P, Cassivi SD, Schild SE, Adjei AA. Non-small cell lung cancer: Epidemiology, risk factors, treatment, and survivorship. Mayo Clin. Proc. 2008; 83:584–594. [PubMed: 18452692]
2. Aberle DR, Adams AM, Berg CD, Black WC, Clapp JD, Fagerstrom RM, Gareen IF, Gatsonis C, Marcus PM, Sicks JD. Reduced lung-cancer mortality with low-dose computed tomographic screening. N. Engl. J. Med. 2011; 365:395–409. [PubMed: 21714641]
3. Bar-Sagi D, Hall A. Ras and Rho GTPases: A family reunion. Cell. 2000; 103:227–238. [PubMed: 11057896]
4. Boettner B, Van Aelst L. The role of Rho GTPases in disease development. Gene. 286
5. Price LS, Collard JG. Regulation of the cytoskeleton by Rho-family GTPases: Implications for tumour cell invasion. Semin. Cancer Biol. 2001; 11:167–173. [PubMed: 11322835]
6. Sahai E, Marshall CJ. RHO-GTPases and cancer. Nat. Rev. Cancer. 2002; 2:133–142. [PubMed: 12635176]
7. Jordan P, Brazåo R, Boavida MG, Gespach C, Chastre E. Cloning of a novel human Rac1b splice variant with increased expression in colorectal tumors. Oncogene. 1999; 18:6835–6839. [PubMed: 10597294]
8. Schnelzer A, Prechtel D, Knaus U, Dehne K, Gerhard M, Graeff H, Harbeck N, Schmitt M, Lengyel E. Rac1 in human breast cancer: Overexpression, mutation analysis, and characterization of a new isoform, Rac1b. Oncogene. 2000; 19:3013–3020. [PubMed: 10871853]
9. Fiegen D, Haeusler LC, Blumenstein L, Herbrand U, Dvorsky R, Vetter IR, Ahmadian MR. Alternative splicing of Rac1 generates Rac1b, a self-activating GTPase. J. Biol. Chem. 2004; 279:4743–4749. [PubMed: 14625275]
10. Matos P, Collard JG, Jordan P. Tumor-related alternatively spliced Rac1b is not regulated by Rho-GDP dissociation inhibitors and exhibits selective downstream signaling. J. Biol. Chem. 2003; 278:50442–50448. [PubMed: 14506233]
11. Radisky DC, Levy DD, Littlepage LE, Liu H, Nelson CM, Fata JE, Leake D, Godden EL, Albertson DG, Nieto MA, Werb Z, Bissell MJ. Rac1b and reactive oxygen species mediate MMP-3-induced EMT and genomic instability. Nature. 2005; 436:123–127. [PubMed: 16001073]
12. Radisky DC. Epithelial-mesenchymal transition. J. Cell Sci. 2005; 118:4325–4326. [PubMed: 16179603]
13. Weinberg RA. Twisted epithelial-mesenchymal transition blocks senescence. Nat. Cell Biol. 2008; 10:1021–1023. [PubMed: 18758491]
14. Stallings-Mann M, Radisky D. Matrix metalloproteinase-induced malignancy in mammary epithelial cells. Cells Tissues Organs. 2007; 185:104–110. [PubMed: 17587815]
15. Radisky DC, Przybylo JA. Matrix metalloproteinase-induced fibrosis and malignancy in breast and lung. Proc. Am. Thorac. Soc. 2008; 5:316–322. [PubMed: 18403326]
16. Illman SA, Lehti K, Keski-Oja J, Lohi J. Epilysin (MMP-28) induces TGF-β mediated epithelial to mesenchymal transition in lung carcinoma cells. J. Cell Sci. 2006; 119:3856–3865. [PubMed: 16940349]
17. McGuire JK, Li Q, Parks WC. Matrilysin (matrix metalloproteinase-7) mediates E-cadherin ectodomain shedding in injured lung epithelium. Am. J. Pathol. 2003; 162:1831–1843. [PubMed: 12759241]
18. Lochter A, Sternlicht MD, Werb Z, Bissell MJ. The significance of matrix metalloproteinases during early stages of tumor progression. Ann. N. Y. Acad. Sci. 1998; 857:180–193. [PubMed: 9917841]
19. Noel A, Boulay A, Kebers F, Kannan R, Hajitou A, Calberg-Bacq CM, Basset P, Rio MC, Foidart JM. Demonstration in vivo that stromelysin-3 functions through its proteolytic activity. Oncogene. 2000; 19:1605–1612. [PubMed: 10734321]
20. Greenlee KJ, Werb Z, Kheradmand F. Matrix metalloproteinases in lung: Multiple, multifarious, and multifaceted. Physiol. Rev. 2007; 87:69–98. [PubMed: 17237343]
21. Collado M, Gil J, Efeyan A, Guerra C, Schuhmacher AJ, Barradas M, Benguria A, Zaballos A, Flores JM, Barbacid M, Beach D, Serrano M. Tumour biology: Senescence in premalignant tumours. Nature. 2005; 436:642. [PubMed: 16079833]

22. Ansieau S, Bastid J, Doreau A, Morel AP, Bouchet BP, Thomas C, Fauvet F, Puisieux I, Doglioni C, Piccinin S, Maestro R, Voeltzel T, Selmi A, Valsesia-Wittmann S, Caron de Fromentel C, Puisieux A. Induction of EMT by twist proteins as a collateral effect of tumor-promoting inactivation of premature senescence. Cancer Cell. 2008; 14:79–89. [PubMed: 18598946]
23. Perl AK, Tichelaar JW, Whitsett JA. Conditional gene expression in the respiratory epithelium of the mouse. Transgenic Res. 2002; 11:21–29. [PubMed: 11874100]
24. Nelson CM, Khauv D, Bissell MJ, Radisky DC. Change in cell shape is required for matrix metalloproteinase-induced epithelial-mesenchymal transition of mammary epithelial cells. J. Cell. Biochem. 2008; 105:25–33. [PubMed: 18506791]
25. Radisky DC, Kenny PA, Bissell MJ. Fibrosis and cancer: Do myofibroblasts come also from epithelial cells via EMT? J. Cell. Biochem. 2007; 101:830–839. [PubMed: 17211838]
26. Shafarenko M, Mahler J, Cochran C, Kisielewski A, Golding E, Wiseman R, Goodrow T. Similar incidence of K-ras mutations in lung carcinomas of FVB/N mice and FVB/N mice carrying a mutant p53 transgene. Carcinogenesis. 1997; 18:1423–1426. [PubMed: 9230291]
27. Kuilman T, Michaloglou C, Mooi WJ, Peeper DS. The essence of senescence. Genes Dev. 2010; 24:2463–2479. [PubMed: 21078816]
28. Tuveson DA, Jacks T. Modeling human lung cancer in mice: Similarities and shortcomings. Oncogene. 1999; 18:5318–5324. [PubMed: 10498884]
29. Lochter A, Galosy S, Muschler J, Freedman N, Werb Z, Bissell MJ. Matrix metalloproteinase stromelysin-1 triggers a cascade of molecular alterations that leads to stable epithelial-to-mesenchymal conversion and a premalignant phenotype in mammary epithelial cells. J. Cell Biol. 1997; 139:1861–1872. [PubMed: 9412478]
30. Lochter A, Srebrow A, Sympson CJ, Terracio N, Werb Z, Bissell MJ. Misregulation of stromelysin-1 expression in mouse mammary tumor cells accompanies acquisition of stromelysin-1-dependent invasive properties. J. Biol. Chem. 1997; 272:5007–5015. [PubMed: 9030563]
31. Gueders MM, Foidart JM, Noel A, Cataldo DD. Matrix metalloproteinases (MMPs) and tissue inhibitors of MMPs in the respiratory tract: Potential implications in asthma and other lung diseases. Eur. J. Pharmacol. 2006; 533:133–144. [PubMed: 16487964]
32. Cichon MA, Gainullin VG, Zhang Y, Radisky DC. Growth of lung cancer cells in three-dimensional microenvironments reveals key features of tumor malignancy. Integr. Biol. 2012; 4:440–448.
33. Uhlen M, Oksvold P, Fagerberg L, Lundberg E, Jonasson K, Forsberg M, Zwahlen M, Kampf C, Wester K, Hober S, Wernerus H, Bjorling L, Ponten F. Towards a knowledge-based Human Protein Atlas. Nat. Biotechnol. 2010; 28:1248–1250. [PubMed: 21139605]
34. Bartling B, Desole M, Rohrbach S, Silber RE, Simm A. Age-associated changes of extracellular matrix collagen impair lung cancer cell migration. FASEB J. 2009; 23:1510–1520. [PubMed: 19109409]
35. Huang Y, Song N, Ding Y, Yuan S, Li X, Cai H, Shi H, Luo Y. Pulmonary vascular destabilization in the premetastatic phase facilitates lung metastasis. Cancer Res. 2009; 69:7529–7537. [PubMed: 19773447]
36. Yeh D, Chen C, Sun MZ, Shao S, Hao L, Song Y, Gong L, Hu J, Wang Q. Caveolin-1 is an important factor for the metastasis and proliferation of human small cell lung cancer NCI-H446 cell. Anat. Rec. 2009; 292:1584–1592.
37. Altin R, Kart L, Tekin I, Armutcu F, Tor M, Ornek T. The presence of promatrix metalloproteinase-3 and its relation with different categories of coal workers' pneumoconiosis. Mediators Inflamm. 2004; 13:105–109. [PubMed: 15203551]
38. Scabilloni JF, Wang L, Antonini JM, Roberts JR, Castranova V, Mercer RR. Matrix metalloproteinase induction in fibrosis and fibrotic nodule formation due to silica inhalation. Am. J. Physiol. Lung Cell. Mol. Physiol. 2005; 288:L709–L717. [PubMed: 15608151]
39. Yamashita CM, Dolgonos L, Zemans RL, Young SK, Robertson J, Briones N, Suzuki T, Campbell MN, Gauldie J, Radisky DC, Riches DW, Yu G, Kaminski N, McCulloch CA, Downey GP. Matrix metalloproteinase 3 is a mediator of pulmonary fibrosis. Am. J. Pathol. 2011; 179:1733–1745. [PubMed: 21871427]

40. Pelisch F, Khauv D, Risso G, Stallings-Mann M, Blaustein M, Quadrana L, Radisky DC, Srebrow A. Involvement of hnRNP A1 in the matrix metalloprotease-3-dependent regulation of Rac1 pre-mRNA splicing. J. Cell Biochem. 2012; 113:2319–2329. [PubMed: 22345078]
41. http://www.nextbio.com.
42. Jorgensen E, Stinson A, Shan L, Yang J, Gietl D, Albino AP. Cigarette smoke induces endoplasmic reticulum stress and the unfolded protein response in normal and malignant human lung cells. BMC Cancer. 2008; 8:229. [PubMed: 18694499]
43. Rangasamy T, Misra V, Zhen L, Tankersley CG, Tuder RM, Biswal S. Cigarette smoke-induced emphysema in A/J mice is associated with pulmonary oxidative stress, apoptosis of lung cells, and global alterations in gene expression. Am. J. Physiol. Lung Cell. Mol. Physiol. 2009; 296:L888–L900. [PubMed: 19286929]
44. Carolan BJ, Harvey BG, De BP, Vanni H, Crystal RG. Decreased expression of intelectin 1 in the human airway epithelium of smokers compared to nonsmokers. J. Immunol. 2008; 181:5760–5767. [PubMed: 18832735]
45. Landi MT, Dracheva T, Rotunno M, Figueroa JD, Liu H, Dasgupta A, Mann FE, Fukuoka J, Hames M, Bergen AW, Murphy SE, Yang P, Pesatori AC, Consonni D, Bertazzi PA, Wacholder S, Shih JH, Caporaso NE, Jen J. Gene expression signature of cigarette smoking and its role in lung adenocarcinoma development and survival. PLoS One. 2008; 3:e1651. [PubMed: 18297132]
46. Kim KK, Kugler MC, Wolters PJ, Robillard L, Galvez MG, Brumwell AN, Sheppard D, Chapman HA. Alveolar epithelial cell mesenchymal transition develops in vivo during pulmonary fibrosis and is regulated by the extracellular matrix. Proc. Natl. Acad. Sci. U.S.A. 2006; 103:13180–13185. [PubMed: 16924102]
47. Johnson L, Mercer K, Greenbaum D, Bronson RT, Crowley D, Tuveson DA, Jacks T. Somatic activation of the K-ras oncogene causes early onset lung cancer in mice. Nature. 2001; 410:1111–1116. [PubMed: 11323676]
48. Thomson S, Buck E, Petti F, Griffin G, Brown E, Ramnarine N, Iwata KK, Gibson N, Haley JD. Epithelial to mesenchymal transition is a determinant of sensitivity of non-small-cell lung carcinoma cell lines and xenografts to epidermal growth factor receptor inhibition. Cancer Res. 2005; 65:9455–9462. [PubMed: 16230409]
49. Witta SE, Gemmill RM, Hirsch FR, Coldren CD, Hedman K, Ravdel L, Helfrich B, D R. Dziadziuszko, Chan C, Sugita M, Chan Z, Baron A, Franklin W, Drabkin HA, Girard L, Gazdar AF, Minna JD, Bunn PA Jr. Restoring E-cadherin expression increases sensitivity to epidermal growth factor receptor inhibitors in lung cancer cell lines. Cancer Res. 2006; 66:944–950. [PubMed: 16424029]
50. Yauch RL, Januario T, Eberhard DA, Cavet G, Zhu W, Fu L, Pham TQ, Soriano R, Stinson J, Seshagiri S, Modrusan Z, Lin CY, O'Neill V, Amler LC. Epithelial versus mesenchymal phenotype determines in vitro sensitivity and predicts clinical activity of erlotinib in lung cancer patients. Clin. Cancer Res. 2005; 11:8686–8698. [PubMed: 16361555]
51. Orlichenko L, Geyer R, Yanagisawa M, Khauv D, Radisky ES, Anastasiadis PZ, Radisky DC. The 19-amino acid insertion in the tumor-associated splice isoform Rac1b confers specific binding to p120 catenin. J. Biol. Chem. 2010; 285:19153–19161. [PubMed: 20395297]
52. Esufali S, Charames GS, Pethe VV, Buongiorno P, Bapat B. Activation of tumor-specific splice variant Rac1b by Dishevelled promotes canonical Wnt signaling and decreased adhesion of colorectal cancer cells. Cancer Res. 2007; 67:2469–2479. [PubMed: 17363564]
53. Matos P, Oliveira C, Velho S, Gonçalves V, da Costa LT, Moyer MP, Seruca R, Jordan P. B-Raf^{V600E} cooperates with alternative spliced Rac1b to sustain colorectal cancer cell survival. Gastroenterology. 2008; 135:899–906. [PubMed: 18602919]
54. Shook D, Keller R. Mechanisms, mechanics and function of epithelial–mesenchymal transitions in early development. Mech. Dev. 2003; 120:1351–1383. [PubMed: 14623443]
55. Mani SA, Guo W, Liao MJ, Eaton EN, Ayyanan A, Zhou AY, Brooks M, Reinhard F, Zhang CC, Shipitsin M, Campbell LL, Polyak K, Brisken C, Yang J, Weinberg RA. The epithelial-mesenchymal transition generates cells with properties of stem cells. Cell. 2008; 133:704–715. [PubMed: 18485877]

56. Reiman JM, Knutson KL, Radisky DC. Immune promotion of epithelial-mesenchymal transition and generation of breast cancer stem cells. Cancer Res. 2010; 70:3005–3008. [PubMed: 20395197]
57. Willis BC, Borok Z. TGF-β-induced EMT: Mechanisms and implications for fibrotic lung disease. Am. J. Physiol. Lung Cell Mol. Physiol. 2007; 293:L525–L534. [PubMed: 17631612]
58. Lu P, Weaver VM, Werb Z. The extracellular matrix: A dynamic niche in cancer progression. J. Cell Biol. 2012; 196:395–406. [PubMed: 22351925]
59. Sympson CJ, Talhouk RS, Alexander CM, Chin JR, Clift SM, Bissell MJ, Werb Z. Targeted expression of stromelysin-1 in mammary gland provides evidence for a role ofproteinases in branching morphogenesis and the requirement for an intact basement membrane for tissue-specific gene expression. J. Cell Biol. 1994; 125:681–693. [PubMed: 8175886]
60. Bernert H, Sekikawa K, Radcliffe RA, Iraqi F, You M, Malkinson AM. Tnfa and Il-10 deficiencies have contrasting effects on lung tumor susceptibility: Gender-dependent modulation of IL-10 haploinsufficiency. Mol. Carcinog. 2003; 38:117–123. [PubMed: 14587096]
61. Festing MF, Lin L, Devereux TR, Gao F, Yang A, Anna CH, White CM, Malkinson AM, You M. At least four loci and gender are associated with susceptibility to the chemical induction of lung adenomas in A/J × BALB/c mice. Genomics. 1998; 53:129–136. [PubMed: 9790761]
62. Lin L, Festing MF, Devereux TR, Crist KA, Christiansen SC, Wang Y, Yang A, Svenson K, Paigen B, Malkinson AM, You M. Additional evidence that the K-ras protooncogene is a candidate for the major mouse pulmonary adenoma susceptibility (Pas-1) gene. Exp. Lung Res. 1998; 24:481–497. [PubMed: 9659579]
63. Nikitin AY, Alcaraz A, Anver MR, Bronson RT, Cardiff RD, Dixon D, Fraire AE, Gabrielson EW, Gunning WT, Haines DC, Kaufman MH, Linnoila RI, Maronpot RR, Rabson AS, Reddick RL, Rehm S, Rozengurt N, Schuller HM, Shmidt EN, Travis WD, Ward JM, Jacks T. Classification of proliferative pulmonary lesions of the mouse: Recommendations of the mouse models of human cancers consortium. Cancer Res. 2004; 64:2307–2316. [PubMed: 15059877]
64. Rice WR, Conkright JJ, Na CL, Ikegami M, Shannon JM, Weaver TE. Maintenance of the mouse type II cell phenotype in vitro. Am. J. Physiol. Lung Cell. Mol. Physiol. 2002; 283:L256–L264. [PubMed: 12114186]

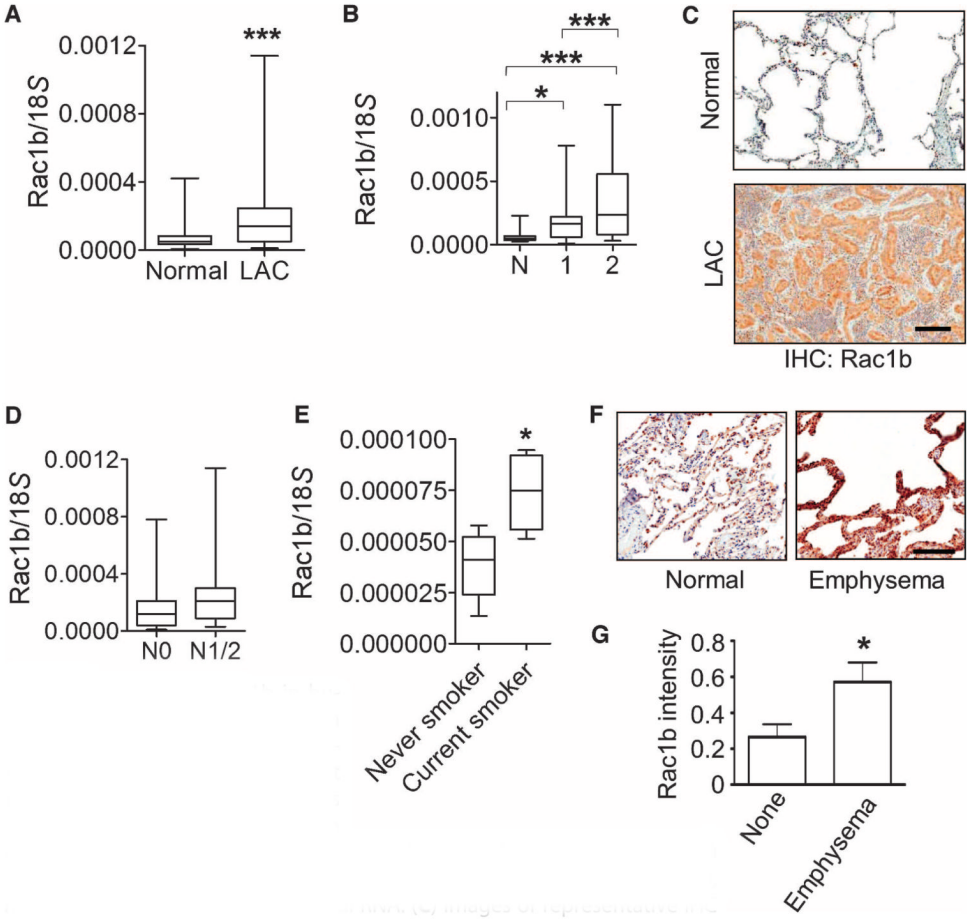

Fig. 1.

Expression of Rac1b in human lung tissue. (**A**) Comparison of Rac1b mRNA expression in human LAC and matched adjacent normal lung tissue homogenates ($n = 68$) by qPCR. (**B**) Comparison of Rac1b mRNA expression by qPCR in biopsies from stage 1 ($n = 32$) and/or stage 2 ($n = 10$) LAC patients with adjacent normal lung tissue (N, $n = 42$), normalized to 18*S* ribosomal RNA. (**C**) Images of representative IHC analyses of the Rac1b protein (brown; Millipore anti-Rac1b, cat. no. 09-271) in LAC ($n = 9$) compared to normal adjacent lung tissue ($n = 4$), indicating staining in epithelial cancer cells. Scale bar, 200 μm. (**D**) Comparison of Rac1b mRNA expression by qPCR in primary tumors of patients with node-negative disease (N0, $n = 42$) and node-positive disease (N1/2, $n = 24$) normalized to 18*S* ribosomal RNA concentrations. (**E**) Comparison of Rac1b mRNA expression by qPCR in lung tumor homogenates from LAC patients identified as current smokers ($n = 4$) and as never smokers ($n = 7$) normalized to 18S ribosomal RNA concentrations. (**F** and **G**) Images of typical IHC analyses (F) and histograms (G) of Rac1b protein staining (brown; Rac1b intensity) in human lung biopsy samples from patients diagnosed with idiopathic pulmonary fibrosis and who displayed peripheral/subpleural distribution of emphysema ($n = 9$) or did not display any axial distribution of emphysema ($n = 11$). Shown are whisker plots indicating data range (whiskers) and interquartile range (boxes) (A, B, D, and E) or averages ± SEM (G). Scale bar, 200 μm. *$P < 0.05$; ***$P < 0.001$; unpaired *t* test (A, B, D, and E) and Mann-Whitney test (G).

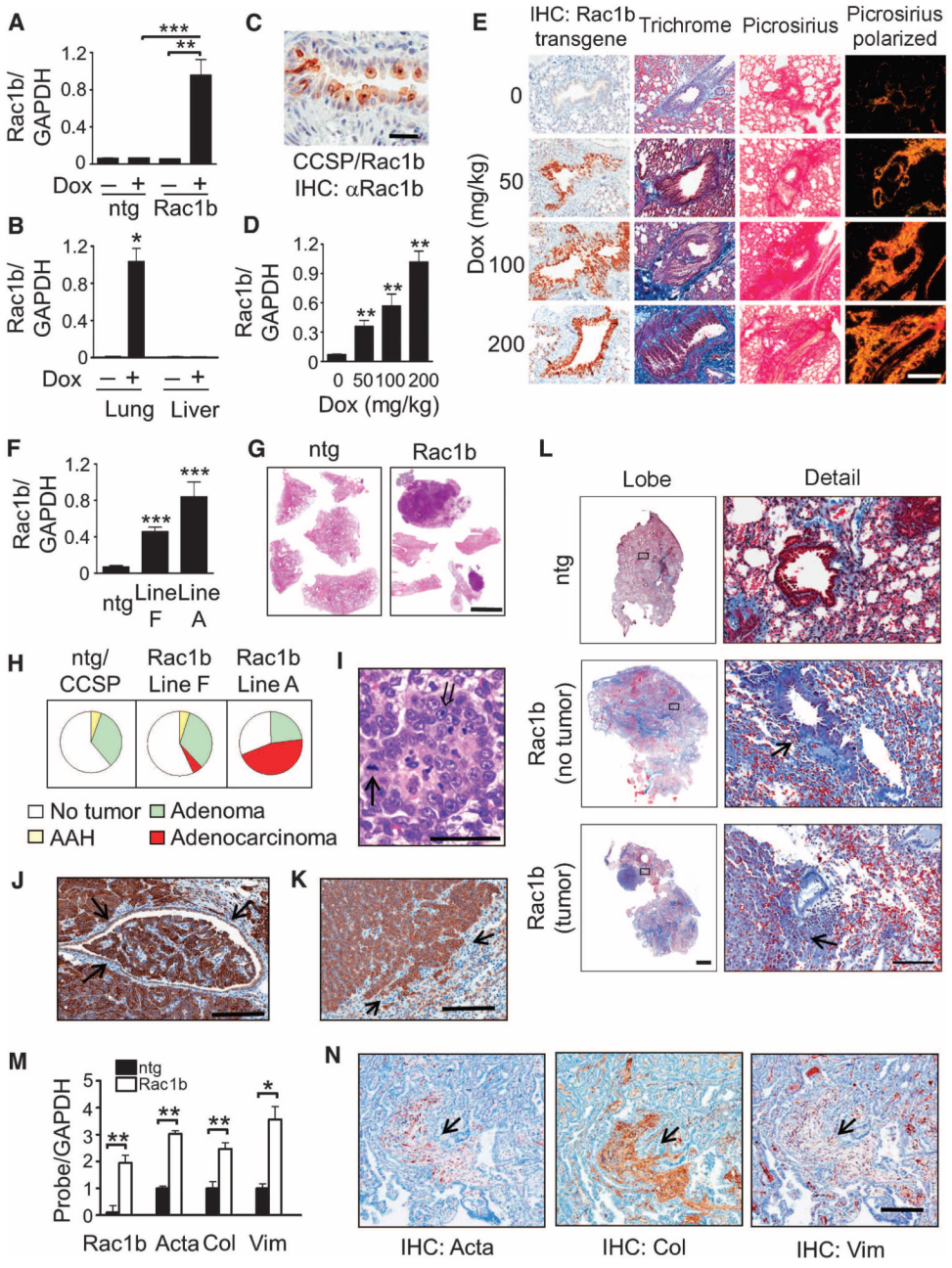

Fig. 2.

Rac1b overexpression in transgenic mouse lung. (**A** to **E**) *tetO-YFP-Rac1b/CCSP-rtta* bitransgenic or *CCSP-rtta* control pups were fed doxycycline for 2 weeks (A to E) either in water (0.5 mg/ml) (A and B) or in feed (200 mg/kg) (C to E). (A) Comparison of Rac1b mRNA expression by qPCR in *tetO-YFP-Rac1b/CCSP-rtta* and *CCSP-rtta* lung homogenates from pups fed ($n = 9$ and $n = 10$, respectively) or not fed ($n = 3$ and $n = 4$, respectively) doxycycline, normalized to glyceraldehyde-3-phosphate dehydrogenase (GAPDH) mRNA concentrations. (B) Comparison of Rac1b mRNA expression by qPCR in *tetO-YFP-Rac1b/CCSP-rtta* ($n = 5$) or *CCSP-rtta* ($n = 3$) lung and liver homogenates, normalized to GAPDH mRNA concentrations. (C) Images of a representative IHC analysis of Rac1b protein staining of lung epithelial cells (brown; $n = 16$) in a bronchiole from a

tetO-YFP-Rac1b/CCSP-rtta mouse. Scale bar, 50 μm. (D) Comparison of Rac1b mRNA expression by qPCR in lung homogenates of mice given doxycycline (Dox) [0 (n = 6), 50 (n = 6), 100 (n = 6), or 200 (n = 4) mg/kg], normalized to GAPDH mRNA concentrations. (E) Images of representative IHC analyses of lung sections from *tetO-YFP-Rac1b/CCSP-rtta* mice given doxycycline (0, 50, 100, or 200 mg/kg). The images show staining of Rac1b transgene expression (brown; custom-made polyclonal anti-Rac1b), collagen deposition with trichrome (blue), and collagen fibril formation with picrosirius red, visualized under bright and polarized light. Scale bar, 200 μm. n = 4 (0 mg/kg Dox); n = 6 (each for 50, 100, and 200 mg/kg Dox). (**F** to **N**) *tetO-YFP-Rac1b/CCSP-rtta* bitransgenic (Line F, n = 23; Line A, n = 13) or *CCSP-rtta* control (ntg; n = 20) mice were fed doxycycline (200 mg/kg) for 60 weeks. (F) Comparison of Rac1b mRNA expression by qPCR in lung homogenates from *tetO-YFP-Rac1b/CCSP-rtta* (Line F, n = 14; Line A, n = 12) or *CCSP-rtta* (n = 7) mice, normalized to GAPDH mRNA concentrations. (G) Representative H&E-stained lung whole-mount sections. Scale bar, 5 mm. ntg, n = 20; Rac1b, n = 36. (H) Distribution and frequency of spontaneously occurring lung tumors in *tetO-YFP-Rac1b/CCSP-rtta* (Line F, n = 23; Line A, n = 13) and CCSP-rtta mice (n = 20). AAH, atypical adenomatous hyperplasia. (I) Representative H&E-stained lung section from an adenocarcinoma observed in a *tetO-YFP-Rac1b/CCSP-rtta* mouse (n = 6). Section shows increased mitosis (arrow) and cytological atypia (double arrow) compared to sporadic adenomas that developed in control *CCSP-rtTA* mice (not shown; n = 7). Scale bar, 50 μm. (J and K) Cytokeratin-stained images of adenocarcinomas observed in *tetO-YFP-Rac1b/CCSP-rtta* mice (n = 6). Scale bar, 200 μm. Images show invasion into an airway (J, arrow) or surrounding alveolar tissue (K, arrow). (L) Representative images of trichrome-stained whole-lung lobes (left column) and details of boxed sections (right column). The images show increased deposition of collagen (blue, arrow) in *tetO-YFP-Rac1b/CCSP-rtta* mice either with (n = 13) or without (n = 6) tumors compared to control *CCSP-rtta* mice (ntg; n = 12). Scale bars, 1 mm (whole lobes) and 100 μm (details). (M) Comparison of Rac1b, smooth muscle actin (Acta), collagen 1α (Col), and vimentin (Vim) mRNA expression by qPCR in whole-lung homogenates from *tetO-YFP-Rac1b/CCSP-rtta* (n = 12) versus *CCSP-rtta* (n = 5) mice, normalized to GAPDH mRNA concentrations. (N) Images of IHC analyses of lung tumor sections from *tetO-YFP-Rac1b/CCSP-rtta* mice (n = 9). The images show intratumoral staining of Acta, Col, or Vim (brown; arrow). Scale bar, 500 μm. *P < 0.05; **P < 0.01; ***P < 0.001, Mann-Whitney test. Shown are averages ± SEM.

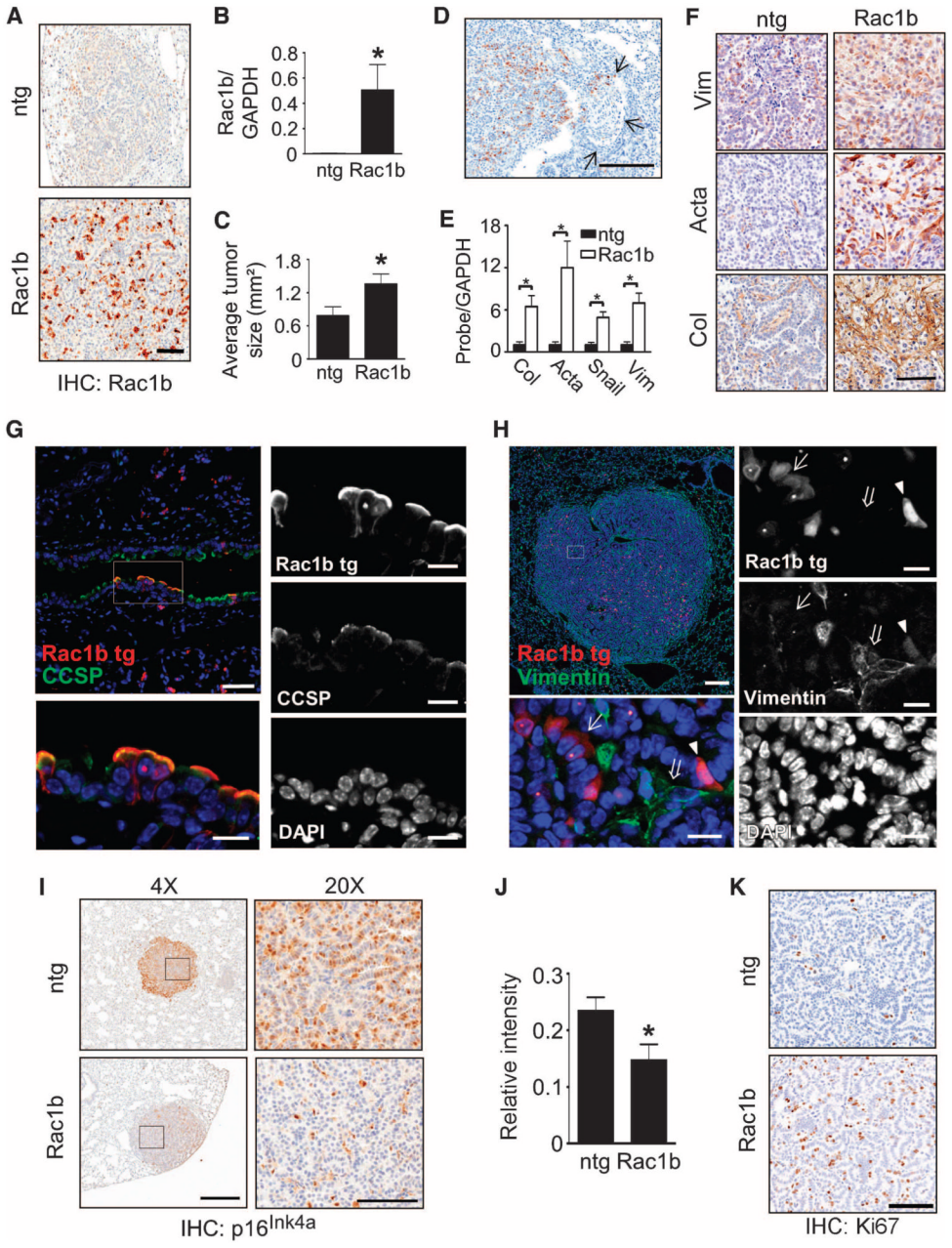

Fig. 3.

Overexpression of Rac1b in urethane-treated transgenic mice. *tetO-YFP-Rac1b/CCSP-rtta* bitransgenic (Rac1b) or *CCSP-rtta* control (ntg) mice were dosed with urethane and fed doxycycline (200 mg/kg) continuously starting at the time of urethane injection. (**A**) Images of IHC analyses of Rac1b protein staining (brown; $n = 9$) in lung tumor sections. Scale bar, 400 μm. (**B**) Comparison of Rac1b mRNA expression by qPCR in lung homogenates from urethane-dosed and doxycycline-fed *tetO-YFP-Rac1b/CCSP-rtta* ($n = 3$) versus *CCSP-rtta* ($n = 5$) mice, normalized to GAPDH mRNA concentrations. (**C**) Histogram showing the average tumor sizes measured from H&E-stained lung sections, comparing tumors ($n = 48$) from *tetO-YFP-Rac1b/CCSP-rtta* mice versus tumors ($n = 22$) from *CCSP-rtta* mice 20 weeks after initiation of urethane dosing. (**D**) Image of green fluorescent protein (GFP)–

stained lung section from a *tetO-YFP-Rac1b/CCSP-rtta* bitransgenic mouse showing an edge of an adenocarcinoma as it invades a neighboring airway (indicated by arrows). Scale bar, 200 μm. (**E**) Comparison of collagen I (Col), smooth muscle actin (Acta), snail, and vimentin (Vim) mRNA expression by qPCR in whole-lung homogenates from *tetO-YFP-Rac1b/CCSP-rtta* ($n = 3$) versus *CCSP-rtta* ($n = 5$) mice, normalized to GAPDH mRNA concentrations. (**F**) IHC images of Vim, Acta, or Col staining in tumor sections from *tetO-YFP-Rac1b/CCSP-rtta* transgenic mice ($n = 4$). Scale bar, 100 μm. (**G**) Representative fluorescence IHC images of co-staining of the *tetO-YFP-Rac1b* transgene product (Rac1b tg, red), the epithelial marker CCSP (green), and nuclei [DAPI (4′,6-diamidino-2-phenylindole); blue] in Clara cells from a *tetO-YFP-Rac1b/CCSP-rtta* transgenic mouse ($n = 2$). Top left, outer view; bottom left and right, magnified views of boxed area in outer view, showing localization of Rac1b tg (top right), CCSP (middle right), DAPI (bottom right), and merged image (bottom left). Scale bars, 50 μm (outer view) and 20 μm (magnified views). (**H**) Representative fluorescence IHC images of co-staining of the *tetO-YFP-Rac1b* transgene product (Rac1 tg, red), the mesenchymal marker vimentin (green), and nuclei (DAPI, blue) in tumor cells from a *tetO-YFP-Rac1b/CCSP-rtta* bitransgenic mouse ($n = 7$). Top left, outer view; bottom left and right panels, magnified views of boxed area in outer view, showing localization of Rac1b tg (top right), vimentin (middle right), DAPI (bottom right), and merged image (bottom left). Arrow, Rac1b tg–expressing epithelial cells; double arrow, vimentin-expressing mesenchymal cells; arrowhead, dual-staining cell undergoing EMT. Scale bars, 200 μm (outer view, top left) and 20 μm (magnified views). (**I** and **J**) Representative immunohistochemical images (I) and histogram (J) of relative $p16^{Ink4a}$ protein staining (brown) in lung tumors from *tetO-YFP-Rac1b/CCSP-rtta* mice ($n = 52$ tumors) versus *CCSP-rtta* mice ($n = 23$ tumors) 14 weeks after initiation of urethane treatment. Scale bars, 500 μm (4×) and 100 μm (20×). (**K**) IHC images of staining for the proliferation marker Ki67 in tumor sections from mice 14 weeks after initiation of urethane treatment ($n = 7$ for each). Scale bar, 100 μm. Shown are averages ± SEM. $^*P < 0.05$, Mann-Whitney test.

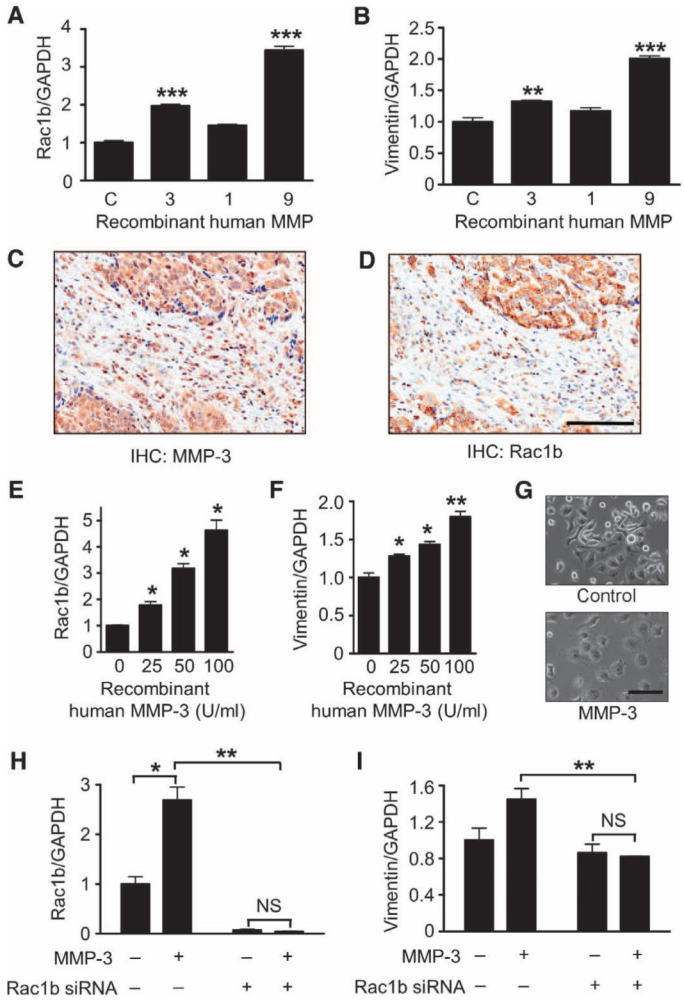

Fig. 4.

MMP-induced expression of Rac1b and vimentin. (**A** and **B**) Comparison of Rac1b (A) and vimentin (B) mRNA expression by qPCR in H661 cell homogenates after treatment for 2 days with no MMP (C) or recombinant human MMP-3, MMP-1, or MMP-9 (0.5 μg/ml; n = 2 per group), normalized to GAPDH mRNA concentrations. (**C** and **D**) Representative IHC images of MMP-3 (C) and Rac1b (D) protein staining (brown) in human LAC patient biopsies (n = 11). Scale bar, 100 μm. (**E** and **F**) Comparison of Rac1b (E) and vimentin (F) mRNA expression by qPCR in H661 cell homogenates before and after treatment for 2 days with recombinant human MMP-3 [0 (n = 2), 25 (n = 2), 50 (n = 3), or 100 (n = 3) U/ml], normalized to GAPDH mRNA concentrations. (**G**) Exposure of H661 cells to recombinant human MMP-3 (100 U/ml) for 2 days induces altered cellular morphology (n = 3 per condition). Scale bar, 50 μm. (**H** and **I**) Comparison of Rac1b (H) or vimentin (I) expression in H661 cell homogenates made from untreated cells and cells that had been transfected with siRNA reagents that selectively target Rac1b in either the presence or the absence of recombinant human MMP-3 (n = 3 per group) (by qPCR, normalized to GAPDH mRNA concentrations). Shown are averages ± SEM. *P < 0.05; **P < 0.01; ***P < 0.001, unpaired t test. NS, not significant.

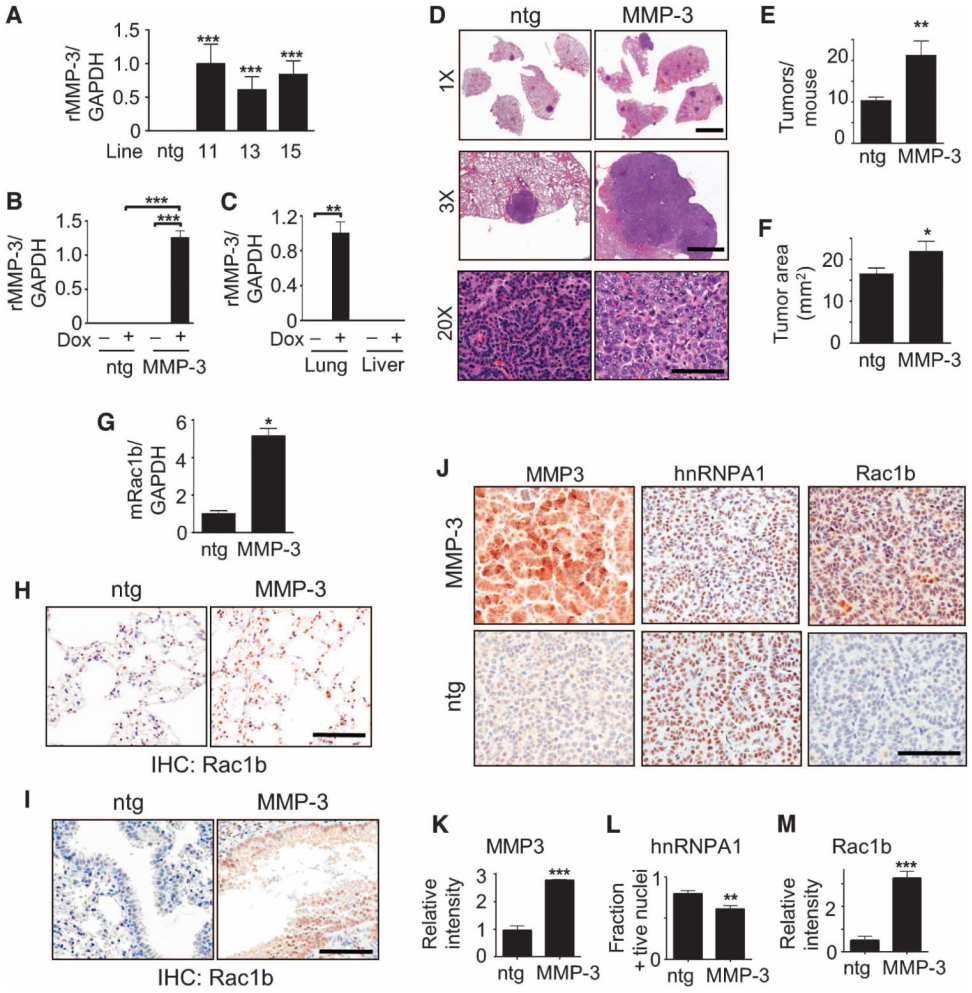

Fig. 5.

Overexpression of MMP-3 in urethane-treated transgenic mice. (**A**) Comparison of MMP-3 transgene expression in lung homogenates from doxycycline-fed *CCSP-rtta* (ntg; $n = 8$) and *tetO-HA-MMP-3/CCSP-rtta* mice [founders 11 ($n = 3$), 13 ($n = 4$), or 15 ($n = 7$)] by qPCR, normalized to GAPDH mRNA concentrations. (**B**) Comparison of MMP-3 transgene expression in lung homogenates from *tetO-HA-MMP-3/CCSP-rtta* (founder 13; MMP-3) and *CCSP-rtta* (ntg) mice fed without ($n = 4$ versus $n = 6$, respectively) or with doxycycline ($n = 3$ versus $n = 5$, respectively) (assessed by qPCR). (**C**) Comparison of MMP-3 transgene expression in lung or liver homogenates from *tetO-HA-MMP-3/CCSP-rtta* [founder 13; MMP-3 (+); $n = 4$] and *CCSP-rtta* [MMP-3 (−); $n = 3$] mice (assessed by qPCR, normalized to GAPDH mRNA concentrations). (**D** to **I**) *tetO-HA-MMP-3/CCSP-rtta* (MMP-3) or *CCSP-rtta* (ntg) mice were fed doxycycline and dosed with 25 mg of urethane weekly for 5 weeks (MMP-3, $n = 6$; ntg, $n = 8$). (D) H&E-stained lung sections at ×1 (scale bar, 5 mm), ×3 (scale bar, 1 mm), and ×20 (scale bar, 200 μm) magnifications. (E) Histogram showing average numbers of tumors present in H&E-stained lung sections from *tetO-HA-MMP-3/CCSP-rtta* (MMP-3) and *CCSP-rtta* (ntg) mice. (F) Histogram showing average sizes of tumors present in H&E-stained lung sections in *tetO-HA-MMP-3/CCSP-rtta* (MMP-3) and *CCSP-rtta* (ntg) mice. (G) Comparison of Rac1b expression in *tetO-HA-MMP-3/CCSP-rtta* (MMP-3) and *CCSP-rtta* (ntg) mice lung homogenates by qPCR, normalized to GAPDH mRNA concentrations. (H and I) Representative IHC images of Rac1b staining (brown) in

alveoli (H) and bronchial airways (I) (MMP-3, $n = 6$; ntg, $n = 8$). Scale bars, 100 μm. (**J**) Representative IHC images of MMP-3 (left column), hnRNP A1 (middle column), and Rac1b staining (right column) from adenomas in *tetO-HA-MMP-3/CCSP-rtta* (MMP-3, top row, $n = 3$) and *CCSP-rtta* (ntg, bottom row, $n = 6$) bitransgenic mice. Scale bar, 100 μm. (**K** to **M**) Histograms showing increased relative stain intensity of MMP-3 (K), decreased fraction of hnRNP A1-positive nuclei (L), and increased relative stain intensity of Rac1b (M) in tumors from tetO-HA-MMP-3/CCSP-rtta bitransgenic mice (MMP-3; $n = 25$) relative to control *CCSP-rtta* (ntg; $n = 9$) mice. $^{*}P < 0.05$; $^{**}P < 0.01$; $^{***}P < 0.001$, unpaired t test (A) and Mann-Whitney test (B, C, E to G, and K to M). Shown are averages ± SEM.

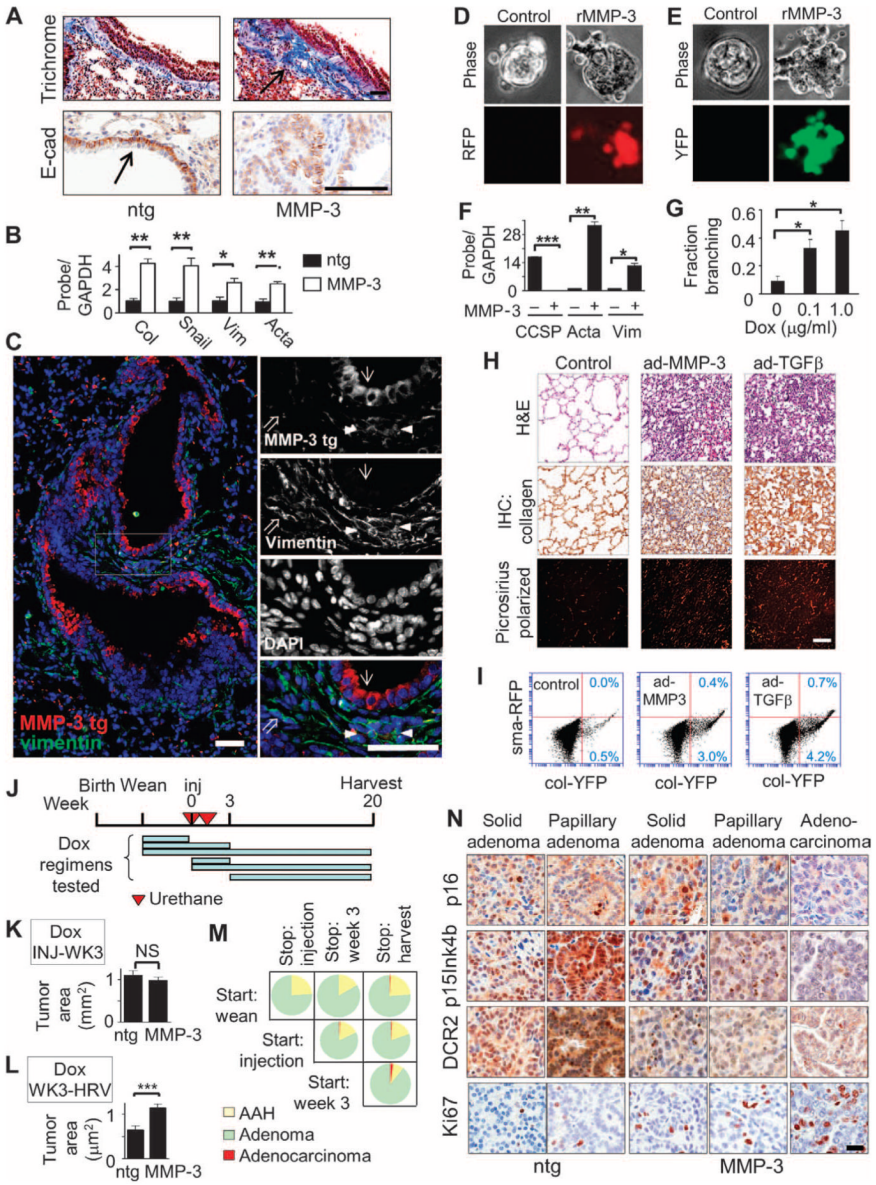

Fig. 6.

MMP-3–driven EMT and senescence bypass during tumor development. (**A**) Images of trichrome staining (top row) indicating collagen deposition (blue) and E-cadherin staining (bottom row) indicating decreased junctional E-cadherin in *tetO-HA-MMP-3/CCSP-rtta* (MMP-3, right column, $n = 17$) and *CCSP-rtta* (ntg, left column, $n = 23$) mice. Scale bar, 100 μm. (**B**) Comparison of collagen (Col), Snail, vimentin (Vim), and smooth muscle actin (Acta) expression in lung homogenates from *tetO-HA-MMP-3/CCSP-rtta* (MMP-3, $n = 6$) and *CCSP-rtta* (ntg, $n = 3$) mice (assessed by qPCR, normalized to GAPDH mRNA concentrations). (**C**) Representative fluorescence IHC images of co-staining of the *tetO-HA-MMP-3* transgene (MMP-3 tg, red), mesenchymal marker vimentin (green), and nuclei (DAPI; blue) in tumor cells from *tetO-HA-MMP-3/CCSP-rtta* bitransgenic mice ($n = 3$). Left, outer view; right, magnified views of boxed area in outer view, showing localization of Rac1b tg (top), vimentin (second), DAPI (third), and merged image (bottom). Arrow, MMP-3 tg–expressing epithelial cells; double arrow, vimentin-expressing mesenchymal

cells; arrow-heads, dual-staining cells undergoing EMT. Scale bars, 50 μm. (**D** and **E**) Representative phase (top rows) and fluorescence (bottom rows) images of primary alveolar epithelial cells isolated from transgenic mice in which RFP expression was controlled by the *smooth muscle actin* promoter (RFP) (D) or from transgenic mice in which YFP expression was controlled by the *collagen 1a1* promoter (YFP) (E). Cells were plated on Matrigel, allowed to adhere for 2 days, and then either left untreated (Control, left columns) or treated with recombinant MMP-3 (rMMP-3, 100 U/ml; right columns) for 4 additional days. Shown is one representative of eight replicate experiments. (**F**) CCSP, Acta, and Vim expression in primary lung epithelial cells cultured on Matrigel and either untreated [MMP-3 (−)] or treated [MMP-3 (+)] with recombinant MMP-3 (100 U/ml) for 4 days (assessed by qPCR, normalized to GAPDH mRNA concentrations) ($n = 2$). (**G**) Histogram showing the fraction of isolated primary lung epithelial cell clusters from *tetO-HA-MMP-3/CCSP-rtta* mice exhibiting branching after treatment with 0, 0.1, or 1.0 μg of doxycycline for 3 days ($n = 2$). (**H**) Representative IHC images showing staining of lung sections for H&E (top row), total collagen (IHC; collagen, brown, middle row), and fibrillar collagen (picrosirius polarized; red, bottom row) from nontransgenic wild-type mice 3 weeks after intratracheal instillation of adenoviruses that expressed the *lacZ* gene [1.0×10^9 plaque-forming units (PFU), control, left column], MMP-3 (1.0×10^9 PFU, ad-MMP-3, middle column), or TGFβ (1.0×10^9 PFU, ad-TGFβ, right column). Scale bar, 100 μm. $n = 5$. (I) Scatter plots of primary epithelial cells isolated from *Col-YFP/Sma-RFP* bitransgenic mice 3 weeks after instillation with adenoviruses that expressed the *lacZ* gene (1.0×10^9 PFU, control, left), MMP-3 (1.0×10^9 PFU, ad-MMP-3, center), and TGFβ (1.0×10^9 PFU, ad-TGFβ, right), sorted by flow cytometry ($n = 5$). (**J**) Diagram of doxycycline administration showing mice dosed with urethane on weeks 1 and 2 where doxycycline was administered at weaning, first injection, or week 3 and withdrawn at injection, week 3, or harvest. (**K**) Histogram showing average sizes of tumors present in H&E-stained lung sections from *tetO-HA-MMP-3/CCSP-rtta* (MMP-3; $n = 8$) and *CCSP-rtta* (ntg; $n = 4$) mice administered doxycycline during urethane administration. (**L**) Histogram showing average sizes of tumors present in H&E-stained lung sections from *tetO-HA-MMP-3/CCSP-rtta* (MMP-3; $n = 11$) and *CCSP-rtta* (ntg; $n = 4$) mice administered doxycycline after urethane administration. (**M**) Distribution and frequency of urethane-induced lung tumors in *tetO-HA-MMP-3/CCSP-rtta* and *CCSP-rtta* mice. AAH, atypical adenomatous hyperplasia. Dox, wean to injection ($n = 6$); wean to week 3 ($n = 8$); wean to harvest ($n = 11$). Dox, injection to week 3 ($n = 8$); injection to harvest ($n = 8$). Dox, week 3 to harvest ($n = 10$). (**N**) Representative IHC images of lung tumor sections from *tetO-HA-MMP-3/CCSP-rtta* (MMP-3; $n = 6$) or *CCSP-rtta* (ntg; $n = 7$) mice showing staining of the senescence markers Cdkn2a (p16), p15Ink4b, and DCR2, or the proliferation marker Ki67 (brown). Scale bar, 50 μm. Shown are averages ± SEM. $*P < 0.05$; $**P < 0.01$; $***P < 0.001$; unpaired *t* test (F and G) and Mann-Whitney test (B, K, and L).